Journal of Applied Electrochemistry (2006) 36:907–912
DOI 10.1007/s10800-006-9164-5


# Electrochemical co-deposition of ternary Sn–Bi–Cu films for solder bumping applications

SHANY JOSEPH[1], GIRISH J. PHATAK[1,*], K. GURUNATHAN[1], TANAY SETH[1], D.P. AMALNERKAR[1] and T.R.N. KUTTY[2]
[1]*Centre for Materials for Electronics Technology (C-MET), Thick Film Materials and Electronic Packaging Group, Panchawati, Off Pashan Road, Pune, 411 008, India*
[2]*Materials Research Centre, Indian Institute of Science, Bangalore, 560012, India*
*(*author for correspondence, tel.: +91-20-2589-8141, fax: +91-20-2589-8085, e-mail: gjp@cmet.gov.in)*

Received 4 January 2005; accepted in revised form 25 April 2006

*Key words:* solder bumping, co-deposition, electroplating, lead-free solders, electronic packaging

**Abstract**

This paper reports the co-deposition of Sn–Bi–Cu films using stannic salt bath which has good stability for up to a week. The effect of current density and bath stirring on the film composition and microstructure has been studied. The deposited films are rich in the more noble metal Bi at current densities up to 5 mA $cm^{-2}$ but stabilize to about 49 wt. % Bi, 47 wt. % Sn and 4 wt. % Cu at 10 mA $cm^{-2}$ and beyond, indicating the effect of limiting current density. There is improvement in the microstructure with stirring or aeration, but the film composition reverts to the Bi rich state, with close to 90 wt. % Bi for deposition at 5 mA $cm^{-2}$. This is attributed to the dispersion of $Sn^{2+}$ ions generated at the cathode during the two-step reduction of $Sn^{4+}$ ions, due to stirring. The bath is suitable for near eutectic compositions of Sn–Bi with $< 5$ wt. % Cu content.

## 1. Introduction

Silicon chips require a large number of Input/Output connections or I/Os due to improved functionality. The chip and package size, at the same time, are required to be kept as small as possible, causing high density of interconnections between chip-package and package-board. Flip chip bonding using solder bumps, which offers the advantage of smaller footprints facilitated by area array interconnections, is fast becoming the preferred interconnection technology [1, 2]. The most common processes for solder bump deposition are evaporation through metal masks, stencil printing and electroplating. The latter process, apart from being widely established and cheap, has an advantage over the other two methods since it can accommodate finer bumps and pitches up to 100 μm or lower due to its compatibility with photolithography [3, 4].

Eutectic tin-lead solder has been the *de facto* standard in the electronic industry for years. Its low melting point, combined with excellent wetting characteristics and good physico-mechanical properties have made Sn–Pb solder almost indispensable for the electronics industry. However, lately, there are concerns over the use of this solder. It is feared that dumping of lead-containing PC boards may contaminate the environment, including drinking water. There is also a possibility of alpha error due to lead in high-density circuits [5]. In view of this, efforts are on to explore and identify suitable "lead-free" alloys which have the best combination of the desired properties, such as, low melting point, good wetting, good shear strength, non-toxicity, good conductivity and low cost, etc. Most of the alloys identified or projected are tin based. The binary and ternary combinations of tin, along with copper and silver are the most sought after alloys. These alloys have a good combination of the desired properties and have been in use for some years in electronic and other applications [5]. Minor additions of elements such as Bi, Co, Sb have been reported to further improve their properties [6–8]. An alloy containing Sn–3.1Bi–3.1Ag–0.5Cu with a melting point in the range 209–212 °C seems to have the best combination of properties [7].

There are some reports on electroplating of lead-free alloys. A few binary and ternary Sn–Ag, Sn–Cu, Sn–Bi and Sn–Ag–Cu co-deposition and sequential deposition systems have been reported [9–14]. In sequential depositions, single or binary/ternary layers are deposited separately and bumps are obtained by reflowing them together. It would always be useful, however, to have a reliable and stable electroplating bath which can deposit all the required elements simultaneously. There are very few reports on electroplating systems for co-deposition of Sn–Bi–Ag–Cu [15]. Nevertheless, we found that a quaternary co-deposition bath with the combination of additives mentioned in this paper is not

stable, possibly because of the reducing nature of Sn ions which leads to the precipitation of Ag ions in the bath. One possible alternative to overcome this difficulty is to electroplate Ag separately and then co-deposit Sn–Bi–Cu. Reflow of these sequentially deposited films would give the desired alloy [16]. The ternary Sn–Bi–Cu deposition system is also complex due to the presence of stannous ions, which may cause precipitation of other ions, especially heavy ions such as Bi. In this paper, we report results of our attempt to electrodeposit Sn–Cu–Bi films using an acidic bath, containing stannic salt as a source of Sn ions. This bath showed good stability. The deposited film composition depends upon the bath chemistry and the deposition conditions such as current density, temperature and bath agitation. This work particularly reports the effect of bath agitation and current density on the film composition and microstructure.

## 2. Experimental

### 2.1. *Substrate preparation*

The electrodepositions were carried out directly on titanium substrates. Titanium was chosen because it is commonly used in solder bumping applications as a barrier layer between Al pads on silicon and solder [1, 3, 17]. In the bump preparation processes reported in the literature [1, 3], an adhesion enhancing layer (Cu) and a diffusion controlling layer (Ni) are also deposited over Ti. However, in this study, the Sn–Bi–Cu films were directly deposited over Ti so that it was compatible for elemental analysis by Energy Dispersive X-ray Spectroscopy (EDS) as the copper substrate would have masked the copper signal arising from the films. The substrates were prepared for plating by first manually polishing them using silicon carbide paper. The substrates were then cleaned with a soap solution and distilled water, followed by degreasing with trichloroethylene in an ultrasonic bath. The substrates were masked using adhesive tapes to define a deposition area of 1 $cm^2$.

### 2.2. *Bath formulation*

The bath formulation for co-deposition of Sn–Cu–Bi comprised of sulphates of Sn, Bi and Cu dissolved in 0.5 M sulphuric acid. $Sn(SO_4)_2$ was prepared using stannic chloride by the following procedure. Stannic hydroxide was first precipitated using $NH_4OH$ and the precipitate was dissolved in sulphuric acid. The remaining salts and other additives were then added and finally the pH was raised. Typically, the bath contained 30 g $l^{-1}$ of $Sn(SO_4)_2$, 2 g $l^{-1}$ of $Bi_2(SO_4)_3$ and 0.2 g $l^{-1}$ of $CuSO_4{\cdot}5H_2O$. Other additives were polycarboxylic acids and EDTA for chelation, surface finishing agents and buffers to finally increase the pH to ~4.5.

*Table 1.* Typical electrodeposition conditions

| S. No. | Parameter | Particulars |
|---|---|---|
| 1 | Current density | 2, 5, 10 & 25 mA $cm^{-2}$ |
| 2 | Temperature | Room temperature |
| 3 | Duration | 60 min |
| 4 | pH | ~4.5 |
| 5 | Bath condition | Static, stirring/aeration |
| 6 | Anode | Carbon |
| 7 | Cathode | Titanium |

### 2.3. *Electrodeposition*

The conditions employed for the electrodeposition experiments are presented in Table 1.

Aeration was done by passing air through the solution using a polypropylene tank with a perforated false bottom. A few electrodepositions were carried out while the solution was stirred using a magnetic stirrer. After deposition, the films were thoroughly rinsed in water, dried and examined.

### 2.4. *Physical and chemical characterization of the bath and the film*

The characterization of the film mainly included thickness measurements, microstructure determination and elemental analyses. The thickness of the films was measured using an optical measuring microscope [Nikon MM-40]. The microstructure and elemental composition of the films were investigated using a Scanning Electron Microscope equipped with an Energy Dispersive X-ray Spectrometer [SEM-EDS, Philips XL-30 with EDAX]. The elemental analyses were based on a standardless evaluation technique. This technique is fairly useful within the known inherent estimation errors that vary depending upon the range of weight content of the individual elements. The estimation errors are as follows:

| Elemental content/wt% | Estimation error/% |
|---|---|
| 20–100 | < 5 |
| 5–20 | < 10 |
| 1–5 | < 20 |
| 0.1–1 | 50–100 |

The cyclic voltametry (CV) of the bath was conducted using a Potentiostat–Galvanostat [PGSTAT 100, Autolab] with a calomel electrode as reference and carbon as the counter electrode.

## 3. Results and discussion

The electroplating bath was found to be stable for about a week after which minor quantities of white precipitate could be seen settling. This is possibly due to precipitation of metastannic acid ($H_2SnO_3$) or $SnO_2 \cdot xH_2O$ [18]. However, the stability is much better when

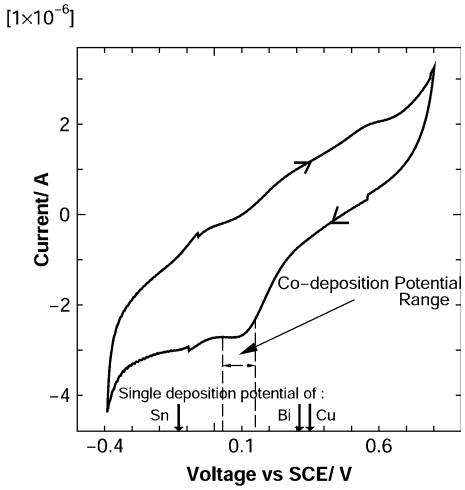


*Fig. 1.* Cyclic voltametry curve for Sn–Bi–Cu bath. The marked 'Single Deposition Potentials' are after Schlesinger and Paunovic [18].

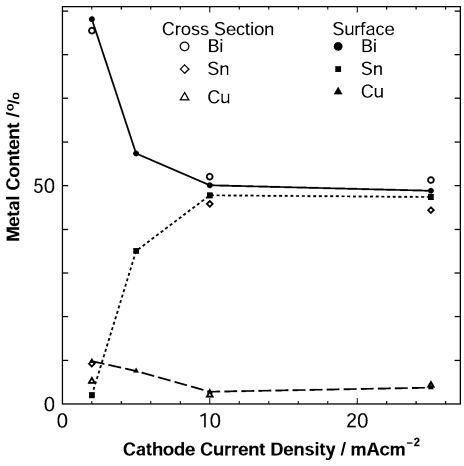


*Fig. 2.* Effect of current density under static bath conditions (without stirring).

compared to baths containing stannous salts and from the point of view of its usage for the intended application. All the depositions were carried out immediately after the preparation of bath. The electrochemistry of the bath was investigated using CV, in order to understand the effect of additives on deposition potentials of constituent metals. Figure 1 presents the CV curve which shows a broad deposition peak between 0.04 V – 0.15 V with no other discernible peaks. The appearance of a single, albeit broad, peak indicates that the additives are effectively modifying the deposition potentials of the constituent metals and bringing them close together. The deposition potentials of the individual elements [18] are also indicated in the Figure 1 for reference. The appearance of a broad reduction peak indicates a complex release mechanism for the ions or unresolved peaks for individual ions. This basic electrochemical analysis, nevertheless, offers sufficient grounds for further investigation of the bath in view of the proposed application.

The films, as deposited using the above bath, had a low thickness of $\sim$5 μm for all the deposition conditions reported here. The average elemental composition of the films on the surface as well as the depths, found from cross-sectional EDS at different current densities is presented in Figure 2. Evidently, when the current density was increased from 2 to 25 mA $cm^{-2}$, the Bi content in the film was reduced from 88 to 49 wt. %. Copper followed a similar trend and its composition decreased from 10 wt. % at 2 mA $cm^{-2}$ to 4 wt. % at 25 mA $cm^{-2}$. Obviously, the composition of Sn in the films increased from 2 wt. % at 2 mA $cm^{-2}$ to 47 wt. % at 25 mA $cm^{-2}$. The accuracy of the Cu content from the standardless elemental estimation by EDS technique was cross-checked by the Inductively Coupled Plasma Optical Emission Spectroscopy (ICP-OES). The copper content was found to be of the same order of magnitude ($<$1 wt. %). Greater accuracy could not be obtained due to dilution errors.

Increase in current density causes the suppression of more noble metals in the deposited film. At a given current density, the rate of deposition of the more noble metal is relatively much closer to its limiting value than that of the less noble metal. An increase in current density, therefore, causes enhanced deposition rate of the less noble metal [19]. At lower current density, the more noble Cu and Bi ions start depositing first as soon as their deposition potentials are reached. At higher current density, the over potentials for all the three elements, i.e., Bi, Cu and Sn increase. It is possible, at current density between 2 and 10 mA $cm^{-2}$, that the reduction of both Bi and Cu ions have reached their limiting current density while the limiting current density for Sn has not been reached. Thus, an increase in current density results in enhanced Sn content in the films. Beyond 10 mA $cm^{-2}$, the reduction of Sn, Bi and Cu have possibly reached their limiting current density. Hence, their composition in the deposited films remains constant even with increasing current density. A similar observation has been made for the depositions of Au/Sn alloy films [20].

The SEM micrographs of the films deposited at different current densities are presented in Figure 3. These static bath depositions indicate non-uniform microstructure for films deposited at lower current density. The non-uniformity gradually reduces with increasing current density. At 25 mA $cm^{-2}$, the microstructure was different with near-spherical grains. Higher current density leads to a fine-grained microstructure due to faster supply of ions which in turn gives rise to formation of new nuclei. Lack of sufficient time for diffusion based grain growth creates fine-grained films [21]. Such a growth can be seen in the micrograph for the film deposited at 25 mA $cm^{-2}$, (Figure 3d). However, gross surface non-uniformity persists for all the current density values.

The cross-sectional elemental analysis of these films reveals chemical composition similar to that on the

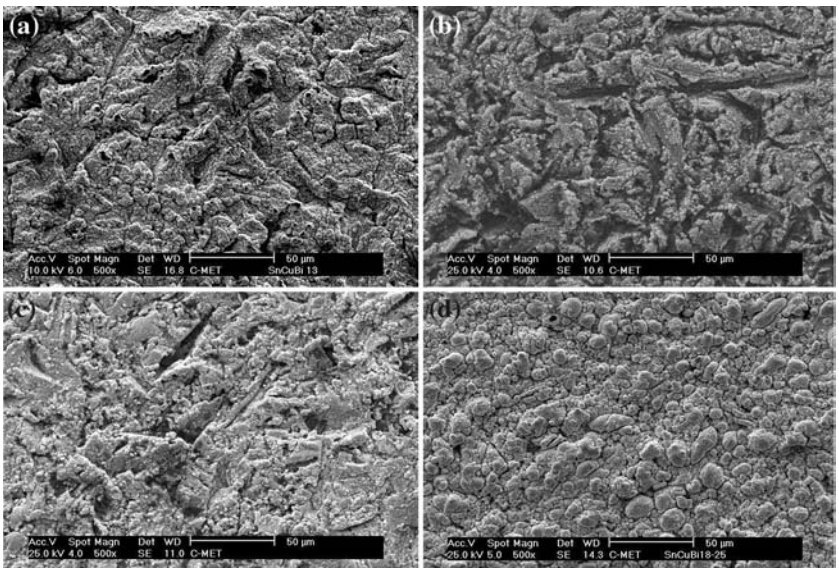


*Fig. 3.* Microstructure of the films deposited under static conditions (without stirring) at (a) 2 mA $cm^{-2}$ (b) 5 mA $cm^{-2}$ (c) 10 mA $cm^{-2}$, (d) 25 mA $cm^{-2}$ current density.

surface. The elemental contents of the film cross-sections plotted in Figure 2 are average values over a few spot analyses at different positions across the width. Figure 4 presents a micrograph of the ''as-sheared'' cross-section of the film deposited at 25 mA $cm^{-2}$. A near-spherical, fine-grained microstructure and thickness in the region of 5 μm is observed.

Table 2 presents the composition of electrodeposited Sn–Bi–Cu films deposited at 5 mA $cm^{-2}$, in static, aerated and stirred condition using a magnetic stirrer. The Sn content in the deposited films under both the stirring conditions falls drastically. While the film deposited using a static bath had 35 wt. % Sn, the films deposited using aerated and stirred baths had only 6–7 wt. % Sn. Further, the results are similar for both stirring methods. The possible reason for this behavior lies in the two-step reaction for Sn deposition:

$$Sn^{4+} + 2e \rightarrow Sn^{2+}$$

$$Sn^{2+} + 2e \rightarrow Sn^{0}$$

Since this reaction occurs near the cathode, the Sn deposition is sensitive to the concentration of $Sn^{2+}$ in the electrode vicinity. The two-step reaction leading to Sn deposition was confirmed by separate, two compartmental electroplating experiments using a porous ceramic membrane container inside the bath. The cathode was placed inside the porous container while the anode was left outside the porous container. The electrolyte from the porous container, which actually represents the solution in the cathodic vicinity was sampled at frequent intervals during the deposition and

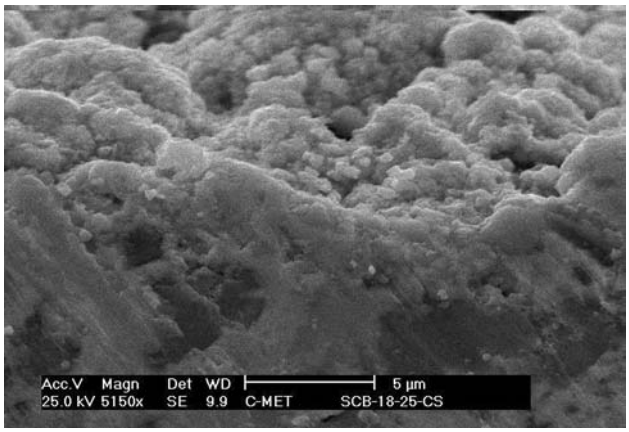


*Fig. 4.* Cross-sectional microstructure of the film deposited at 25 mA $cm^{-2}$ under static conditions (without stirring).

*Table 2.* Composition of the films deposited under static & stirring conditions

| S. No. | Stirring condition | Composition/wt. % at 5 mA $cm^{-2}$ | | |
|---|---|---|---|---|
| | | Sn | Bi | Cu |
| 1 | Static | 35 | 57 | 8 |
| 2 | Aerator | 5 | 90 | 5 |
| 3 | Magnetic stirring | 3 | 90.5 | 6.5 |

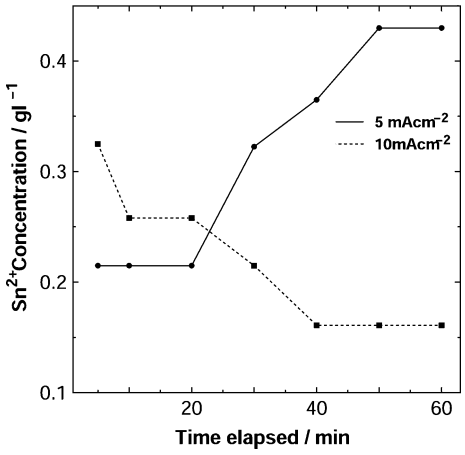


*Fig. 5.* Concentration of $Sn^{2+}$ in the two compartment electroplating bath vs time during depositions at 5 & 10 mA $cm^{-2}$.

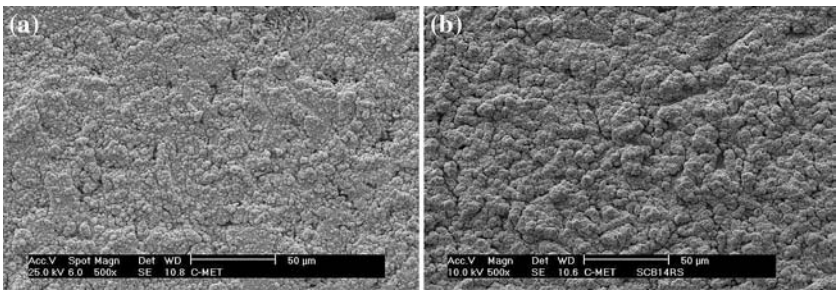


*Fig. 6.* Microstructure of films deposited at 5 mA $cm^{-2}$ under (a) aeration, and (b) magnetic stirring.

analyzed for stannous ion concentration by titrating against 0.0167 M potassium iodate solution using starch solution as the indicator. The concentration of $Sn^{2+}$ ions in the vicinity of the cathode during the deposition for 5 and 10 mA $cm^{-2}$ is shown in Figure 5. It is seen that the concentration of $Sn^{2+}$ as a function of time increased for the deposition at 5 mA $cm^{-2}$ and decreased for the deposition at 10 mA $cm^{-2}$. It is noted that aquated $Sn^{2+}$ ions do not occur in solutions. $Sn^{2+}$ is found in various forms including $Sn(OH)^{+}$, $Sn(OH)^{2+}$, $Sn(OH)_2^{2+}$ and $Sn(OH)_3^{-}$ [22]. In presence of sulphate, cationic as well as anionic species may prevail, e.g. $[Sn(OH)_4]^{2+}$, $[Sn(OH)_2SO_4]^{2-}$. These species may be further modified by chelating agents. As a result of the complex ion formation $Sn^{2+}$ to $Sn^0$ conversion requires higher activation energy. The activation barrier may be diminished only at higher current densities. But for the complex ion formation, the stannous ions could be easily oxidized during stirring in air by aeration since the redox potential:

$Sn^{2+} \rightarrow Sn^{4+} + 2e$; $E^0 = 0.15$ V is relatively lower. Nevertheless, the change in $Sn^{2+}$ concentration as the deposition progressed confirms that Sn deposition is preceded by the cathodic reactions mentioned above. These $Sn^{2+}$ ions tend to accumulate near the electrode if the free movement of electrolyte is restricted. When not restricted, the $Sn^{2+}$ concentration would fall of to near zero away from the electrode. Under stirring conditions this fall off should be much faster as compared to the static conditions. If vigorously stirred, the peak concentration of $Sn^{2+}$ ions, close to the electrode, may also decrease.

The microstructures of the films deposited from aerated and stirred baths are shown in Figure 6. As expected, the uniformity and compactness of the films shows improvement due to stirring by either method, though some voids are seen on the surface. Overall, there is significant improvement in microstructure due to stirring.

## 4. Conclusions

Films with ~5 μm thickness and a composition of 49Bi–47Sn–4Cu were obtained using the present bath under unstirred, static conditions, which changed to low tin containing composition of ~90Bi–5Sn–5Cu under stirring conditions. The compositional uniformity of the films across the volume was confirmed by cross-sectional EDS analysis. Although the cyclic voltametry indicated the possibility of multi-element co-deposition, the composition of the films was much different from the targeted high tin alloy. This could be due to the complex release mechanism of the metal ions from the chelates, which possibly ensures close but different deposition potentials. The Sn content was found to be controlled by its two-step reduction at the cathode. A comparatively low concentration $Sn^{2+}$ near the cathode explains low growth rates. Use of appropriate reducing agents for reduction of stannic ions to the stannous state might alter the composition of the deposited films. The present bath, however, shows suitability for the near eutectic composition of Sn–Bi with minor amounts of Cu.

## References


1. P.A. Totta, S. Khadpe, N.G. Koopman, T.C. Reiley and M.J. Sheaffer, *in* R.R. Tummala, E.J. Rymaszewski, A.G. Klopfenstein (eds), Chip-To-Package Interconnections in Microelectronics Packaging Handbook, Vol. II (Chapman. & Hall, Newyork, 1997), pp. 136–144.
2. G. R. Blackwell, The Electronic Packaging Handbook (CRC press & IEEE press, 1999) 4.4–4.6 pp.
3. J.H. Lau, *Flip Chip Technologies* (Mc Graw-Hill, New York, 1996).
4. J.H. Lau, *IEEE Trans. Electron. Packag. Manufac.* **23** (2000) 4.
5. J.H. Lau and S.W.R. Lee, *Microvias for Low Cost High Density Interconnects* (McGraw Hill, N.Y., 2001), pp. 332–359.
6. K. Seeling and D. Suraski, The status of lead-free solder Alloys, Proceedings of 50th Electronic Components and Technology Conference (ECTC), Las Vegas, U.S.A., 21–24 May 2000, IEEE pp. 1405–1409.
7. J.S. Hwang, *Bismuth in Electronic Solder (Part 1) Bull Bismuth Inst* **78** (2001) 1.
8. I.E. Anderson, J.C. Foley, B.A. Cook, J. Harringa, R.I. Terpstra and O. Unal, *J. Electron. Mater.* **30** (2001) 1050.
9. S. Arai, H. Akatsuku and N. Kaneko, *J. Electrochem. Soc.* **150** (2003) C730.
10. C.E.W. Ming and Z.S. Karim, US Patent No. 6,638,847 (Oct. 2003).
11. H. Ezawa, M. Miyata, S. Honma, H. Inoue, T. Tokuoka, J. Yoshioka and M. Tsujimura, Eutectic Sn-Ag solder Bump process for ULSI flip chip technology, Proceedings of 50th Electronic Components and Technology Conference (ECTC), Las Vegas, U.S.A., 21–24 May 2000, IEEE, pp. 1095–1100.
12. S.D. Beattie and J.R. Dahn, *J. Electrochem. Soc.* **150** (2003) 457.
13. K. Gurunathan, S. Joseph, D.R. Yewale, A.N. Phalke, T. Seth, G.J. Phatak, D.P. Amalnerkar and T.R.N. Kutty, *Trans SAEST* **37** (2002) 127.
14. K. Bioh and T. Ritzdorf, *J. Electrochem. Soc.* **150** (2003) 253.
15. H. Sakurai, A. Saito, M. Date and O. Mita, US Patent No. 5,759,381 (June 1998).

16. S. Joseph, G.J. Phatak, T. Seth, K.Gurunathan, D.P. Amalnerkar and T.R.N. Kutty, Lead-free Solder Bumping by Electroplating Process for Electronic Packaging., Proceedings of IEEE TENCON Conference, 15–17 Oct. 2003, Bangalore, India Vol. IV, pp. 1367–1371.
17. C.J. Chen and L. Kwag-Lung, *J. Electron. Mater.* **29** (2000) 1007.
18. M. Schlesinger and M. Paunovic, Modern Electroplating (Wiley-Interscience Publication, 2000), 257 pp.
19. A. Brenner, Electrodeposition of Alloys: Principles and Practice, Vol. 1, (Academic Press, 1963), 123 pp.
20. A. He, B. Djurfors, S. Akhlaghi and D.G. Ivey, *Plating Surf. Finish.* **89** (2002) 48.
21. N.V. Partha Sarathy, Practical Electroplating Handbook (Prentice Hill Publication, 1981), 54 pp.
22. M. Pettine, F.J. Millero and G. Macchi, *Anal. Chem.* **53** (1981) 1039.